Influence of molecular ordering on electrical and friction properties of ω-(*trans*-4-stilbene)alkylthiol self-assembled monolayers on Au (111)

Yabing Qi [1,2,*], Xiaosong Liu [3], B.L.M. Hendriksen [2], V. Navarro [2], Jeong Y. Park [2], Imma Ratera [2,$], J. M. Klopp [4], C. Edder [4], Franz J. Himpsel [3], J.M.J. Fréchet [4,5], Eugene E. Haller [2,6], and Miquel Salmeron [2,4,6]

[1]Applied Science and Technology Graduate Group, University of California, Berkeley CA 94720
[2]Materials Sciences Division, Lawrence Berkeley National Laboratory, University of California, Berkeley CA 94720
[3]Department of Physics, University of Wisconsin-Madison, Madison, WI 53706
[4]The Molecular Foundry, Lawrence Berkeley National Laboratory, University of California, Berkeley CA 94720
[5]Department of Chemistry, University of California, Berkeley CA 94720
[6]Department of Materials Sciences and Engineering, University of California, Berkeley CA 94720

The electrical and friction properties of ω-(*trans*-4-stilbene)alkylthiol self-assembled monolayers (SAMs) on Au(111) were investigated using atomic force microscopy (AFM) and near edge x-ray absorption fine structure spectroscopy (NEXAFS). The sample surface was uniformly covered with a molecular film consisting of very small grains. Well-ordered and flat monolayer islands were formed after the sample was heated in nitrogen at 120 °C for 1 h. While lattice resolved AFM images revealed a crystalline phase in the islands, the area between islands showed no order. The islands exhibit substantial reduction (50%) in friction, supporting the existence of good ordering. NEXAFS measurements revealed an average upright molecular orientation in the film, both before and after heating, with a narrower tilt-angle distribution for the heated fim. Conductance-AFM measurements revealed a two orders of magnitude higher conductivity on the ordered islands than on the disordered phase. We propose that the conductance enhancement is a result of a better π-π stacking between the *trans*-stilbene molecular units as a result of improved ordering in islands.

*Current address: Department of Electrical Engineering, Princeton University, Princeton, NJ 08544. E-mail: yabingqi@gmail.com.
$Current address: Department of Molecular Nanoscience and Organic Materials, Institut de Ciència de Materials de Bacelona (ICMAB-CSIC), Bellaterra, 08193, Spain

1. Introduction

Conductive organic polymers and oligomers have been continuing to attract attention because of their potential applications in organic electronics and molecular devices. [1-5] Poly(p-phenylene vinylene) (PPV) is one of the most extensively studied conductive polymers that exhibit potential applications in opto-electronic devices. [6-10] The importance of conjugation to conduction has been illustrated by Giro et al. by incorporating a fully conjugated polymer (PPV) into a poly(p-phenylene) chain, which gave rise to an intermediate band gap depending on the PPV concentration [9]. Stilbene is the shortest "model" oligomer (OPV) of PPV. Upon ultraviolet irradiation, stilbene can be transformed reversibly between two isomeric configurations: *trans* and *cis*-stilbene. [11] The light-induced mechanical switching of single molecules of a similar molecule - azobenzene - has also been observed by atomic force microscopy (AFM) [12], scanning tunneling microscopy (STM) [13-15], and photoemission spectroscopy [16]. It was proposed that these conformational transitions can be used as a molecular switch [17].

Ruini et al. reported that the interchain interactions and the crystal structure of PPV crystals could play an important role in modifying exciton states and optical properties. [10] In molecular systems containing π orbitals, the orientation and packing of the molecules in monolayers are critical for charge transport by providing intermolecular π-coupling. Seferos et al. studied electronic coupling via π-π interactions using a crossed-wired tunnel junction. [18] They compared the conduction across monolayers of two molecules: one containing a π-conjugated framework - OPV3 (an oligomer consisting of three phenylene vinylene units), the other containing a pair of stilbene units attached through an ethylene bridge - a [2.2] paracyclophane (pCp) core. The cofacial ring-ring stacking imposed by the pCp core in the second molecule provided strong through-space π-π coupling that is efficient at promoting charge transport across the system. Finally the chemical bond to the substrate is important. For example, Danilov et al. observed the bistability in the current-voltage (IV) characteristics of single-molecule junctions containing OPV3, and attributed it to breaking and reformation of S-Au bonds. [19] Similarly Ranganathan et al. reported a switching behavior in the IV curves of a nitroazobenzene junction. [20]

Hybrid molecules consisting of a saturated chain and a functional group are appealing because of their ability to form well-ordered films and the possibility of modifying their functionality by tailoring the embedded groups. While the conduction mechanism in self-assembled monolayers (SAMs) of non-conjugated alkanethiol has been extensively studied, [21-23] understanding of electron transfer taking place in these hybrid molecules still remains elusive.

Alkanethiol SAMs have been investigated for their friction and lubrication properties. The strong binding to substrates, ease of preparation, and versatility in tailoring film parameters make SAMs attractive candidates. The nanotribological properties of SAMs have become the subject of many studies [24-28].

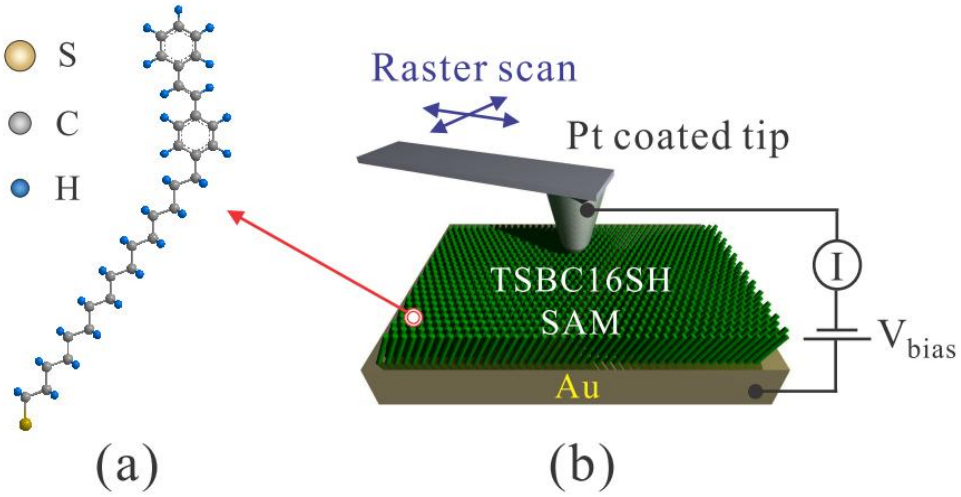

Figure 1: Schematic representations of (a) ω-(*trans*-4-stilbene)hexadecanethiol and (b) conductance atomic force microscopy setup.

In this article we report a combined AFM and near edge x-ray absorption fine structure spectroscopy (NEXAFS) study of the electrical and mechanical properties of a *trans*-stilbene based molecule: ω-(*trans*-4-stilbene)hexadecanethiol (TSBC16SH), schematically shown in Fig. 1a. Alkanethiols are well known to form densely-packed well-ordered SAMs on Au(111). The *trans*-stilbene tail group allowed us to investigate its effect on the electrical and mechanical properties (in particular friction) of monolayer thin films. Understanding the role of the conjugated groups and of the saturated chains can give insight in designing and engineering molecular assemblies [9,29,30].

2. Experiment

All chemicals were purchased from Aldrich and used without further purification. The synthesis procedure of TSBC16SH molecules is given in the Supporting Information.

Gold films (150 nm thick) were produced by evaporating the metal onto a freshly cleaved mica substrate at a pressure of 10^{-6} Torr. The Au/mica samples were then flame annealed using a butane torch shortly before SAM preparation. The resulting surface exhibits flat (111) terraces with sizes up to 500 nm separated by monatomic steps. The molecular films were self-assembled by immersing the substrates in a cyclohexane solution of TSBC16SH with a concentration 1 mM for 12 hours, followed by rinsing in pure cyclohexane and drying with nitrogen gas. Post-annealing of the samples at 120 °C was performed in an oven in a nitrogen gas atmosphere.

Experiments were performed using a commercial AFM from Agilent [31] in air. For high-resolution imaging, Si_3N_4 cantilevers with nominal spring constants of 0.12 N/m were used. [32] For conductance-AFM (C-AFM) measurements, Si cantilevers with nominal spring constants of 0.2 N/m coated with approximately 5 nm of chromium and 15 nm of platinum [33] were used. The cantilever spring constants were calibrated using the resonance-damping method of Sader et al. [34] During C-AFM measurements the sample was clamped with a Cu spring, which served to provide the bias voltage. Current and friction force were simultaneously recorded while normal force was kept constant (Fig.

1b). The load used in this study was sufficiently low to keep the deformation of SAMs in the elastic region. Subsequent inspection of AFM images confirmed that no detectable damage to the SAM was produced, except for the image presented in Fig. 6, in which a high normal force was applied during scanning to investigate its effect on the electrical properties of the film.

Total electron yield (TEY) and fluorescence yield (FY) NEXAFS spectra of the C 1s edge were acquired at Beamlime 8.0 of the Advanced Light Source (ALS) in Lawrence Berkeley National Laboratory (LBNL). The TEY signal was collected by measuring the sample photocurrent while the fluorescence yield data was acquired using a microchannel plate with an Al filter. The normalization with respect to the incident photon flux was achieved by simultaneous measurement of the photocurrent from an upstream Au grid. To lower the radiation damage the measurements were preformed with a defocused spot and narrow slits. Several spectra were collected at different spots on each sample to confirm the sample homogeneity. Normalization of the spectra was performed following standard procedures: A linear background, which accounts for absorption from the substrate and from valence states, was subtracted from the spectra by fitting to the pre-edge energy region. The resulting spectra were normalized to a common step height between the pre-edge and the post-edge regions, which makes them proportional to the absorption per carbon atom.

3. Results

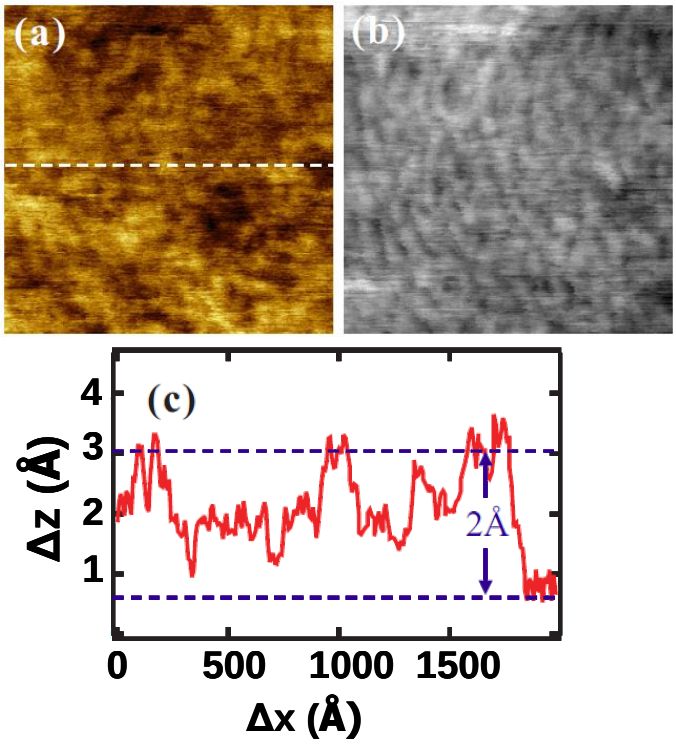

Figure 2. 200 nm × 200 nm tapping-mode AFM topographic (a), and phase images (b) of a freshly prepared TSBC16SH SAM on Au(111), prior to heating (scanning speed = 800 nm/s). (c) Height profile along the dashed line in (a).

Fig. 2a shows a tapping-mode AFM topographic image of a freshly prepared TSBC16SH SAM on Au(111) before annealing. The surface consists of small grains, 10 to 20 nm in size, which are more clearly visible in the phase image (Fig. 2b). The topographic variation from the top of the domains to the valleys in between is ~ 2 Å as can be seen from the height profile (Fig. 2c). Similar grain features were also observed in contact mode AFM images. The presumably strong interaction of the *trans*-stilbene (TSB) unit with the surface makes it possible for some molecules to lie flat on the surface. Indeed an STM study of a similar molecule with a much shorter alkyl chain (TSBC1SH) shows that the molecules prefer to lie flat on the Au(111) surface [35]. In our case the Van der Waals force between the long alkyl chains causes most of the TSBC16SH molecules to assume a more vertical orientation [36]. Another effect of the TSB group is to make sterically difficult the growth of long range order at room temperature [36-38]. Indeed we could not observe molecular lattice resolution prior to heating in our images. Concomitant with the lack of long range order in the non-annealed TSBC16SH is the very low current level (< 1 pA) detected, for bias voltages of up to 3V. When a bias larger than 3V is applied, the molecules undergo irreversible electrical breakdown, leading to a sudden current jump.

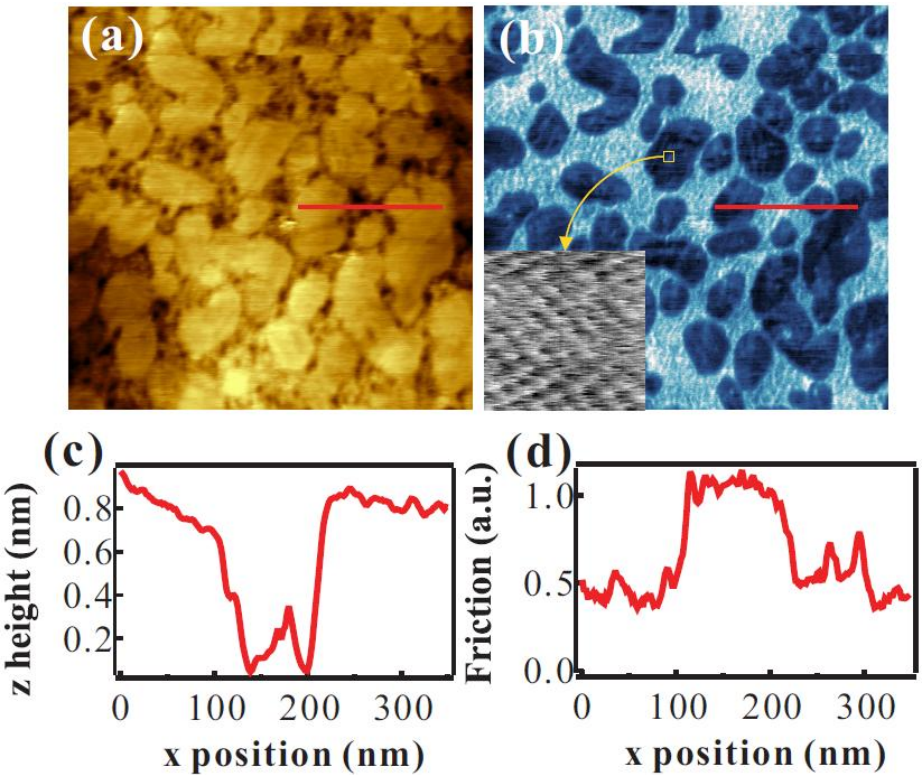

Figure 3. 1 µm × 1 µm contact-mode AFM (a) topographic, and (b) friction images (bright is high and dark is low friction) acquired under a total load of 5.5 nN. The sample was annealed for 1 hour at 120 °C in N_2 gas. (c) and (d) are profiles along the marked lines in (a) and (b), revealing a 50% reduction in friction on islands due to good molecular ordering. The inset in (b) is a 4 nm × 4 nm lattice resolved friction image on top of large islands (scanning speed = 2.6 µm/s).

When the sample was heated in a nitrogen gas atmosphere at 120 °C for 1 h flat islands with sizes in the range of 100 to 200 nm were formed, separated by gaps about 8 Å deep, as can be seen from Fig. 3a. These islands have a smooth morphology with a height variation of ~ 0.5 Å. The area between islands is covered with disordered molecules (referred as the disordered phase hereafter) with a topographical RMS roughness as high as ~ 4 Å, which is rougher than the surface of the non-annealed samples (RMS roughness ~ 2 Å). The fact that the topographic height of the islands is larger than that of the surrounding disordered phase by ~ 6 Å indicates that the disordered phase must have a higher degree of molecular tilt on the surface. The friction force on large islands is only 50% of that on the disordered phase (Fig. 3d). This result is consistent with a lesser degree of ordering in the disordered phase. It has been proposed that in addition to induce ordering, heating also produces desorption, which creates extra space for molecules to assume larger tilt angles. This is possibly the cause of the increased roughness in the disordered phase [39]. In a well-packed molecular lattice the molecules have less freedom to move due to strong inter-molecular interactions. This quenches energy dissipation modes such as molecular tilting, rotations and gauche defects, which results in a reduction of friction [40]. While lattice resolved AFM images could be obtained on the islands (see inset in Fig. 3b), they could not be obtained on the disordered phase under the same imaging conditions. By comparing the topographic and friction images, it is interesting to notice that the apparent lateral size of the islands is ~ 20% larger in the topographic image than that in the friction image. This is caused by tip convolution, a common artifact in scanning probe microscopy imaging. When the tip comes to the edge of the island, instead of an abrupt decrease in height, a rather gentle slope is observed (Fig. 3c) because of the large radius of the tip. On the other hand, the friction is very sensitive to the ordering of molecules. At the edge of large islands a substantial disorder is expected, so the friction profile is much steeper at the edge of large islands (Fig. 3d). [40-42]

In order to characterize the orientational configuration of the molecules in the SAM, we performed NEXAFS on the C 1s edge, both in total electron yield (TEY) and in fluorescence yield (FY) modes. The TEY spectra of TSBC16SH SAM before and after annealing are shown in Fig. 4a and b, respectively. The fluorescence yield data (not shown) show similar features. Four core-to-valence transitions of the C 1s into empty orbitals are labeled. Peak 1 corresponds to a transition to the anti-bonding orbital $\pi_1^*{}_{C=C}$. Peak 2 corresponds to a transition to the anti-bonding orbital σ^*_{C-H}. Peak 3 is assigned to a transition to the higher-lying anti-bonding orbital $\pi_2^*{}_{C=C}$. Peak 4 corresponds to a transition to the anti-bonding orbital σ^*_{C-C}. [43,44] There is no obvious difference in the position of these absorption peaks in the spectra of unannealed and annealed SAMs, which indicates no chemical change caused by annealing process.

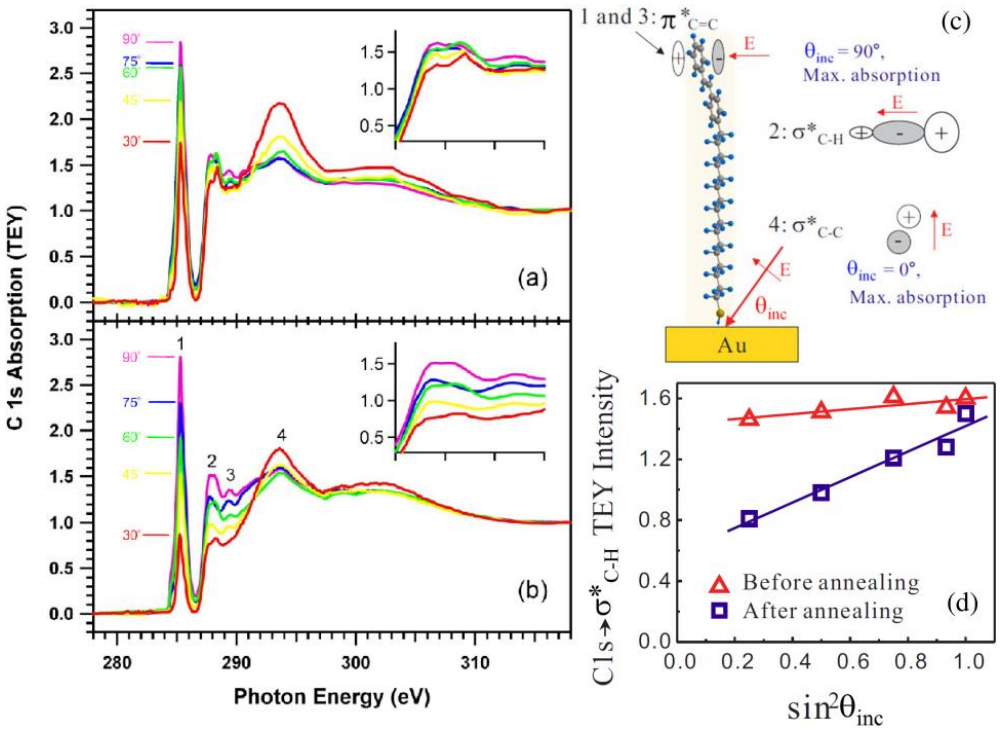

Figure 4. C 1s NEXAFS spectra of TSBC16SH SAMs prior to heating (a), and after heating (b) for various polarization angles θ (90° to 30°). The angle θ is that between the incident x-ray and the sample surface, so that θ = 90° corresponds to normal incidence. A strong polarization orientation dependence of C 1s to π^*, σ^* transitions is observed, particularly after annealing. (c) Schematics of the NEXAFS geometry. (d) Polarization dependence of the intensity of C 1s to $\sigma^*_{C\text{-}H}$ in the TSBC16SH SAM before (red triangle) and after (blue square) annealing.

NEXAFS measures optical dipole transitions from a core level to unoccupied valence orbitals. By using the linearly polarized light of the synchrotron, the spatial orientation of the orbitals can be in principle determined from the dipole selection rules and the observed angular dependence of the transition intensity. For the simple s-to-p transition, the observed intensity is maximum if the electric field vector E of incident x-ray is parallel to the transition dipole moment p, and follows the $\cos^2\theta_E$ relation, where θ_E is the angle between vectors E and p. In this study spectra were recorded at angles θ_{inc} = 30°, 45°, 60°, 75°, 90°, where θ_{inc} is the angle between the incident x-ray beam and the sample surface, which is the angle between the photon electric field vector (E) and the sample normal. The intensity of transitions from C 1s to $\sigma^*_{C\text{-}C}$ (peak 4) decreases with increase in the angle θ_{inc} from 30° to 90°. On the contrary, the intensity of transitions from C 1s to $\sigma^*_{C\text{-}H}$ (peak 2) increases with increase in the angle θ_{inc}. This result indicates that the C-C bonds are tilted closer to the surface normal whereas the C-H bonds are more parallel to the surface. The intensity of transitions from C 1s to $\pi_1{}^*_{C=C}$ (peak 1) follows the same trend as C 1s to $\sigma^*_{C\text{-}H}$ transitions, which indicates that the aromatic rings are mostly on a plane perpendicular to the sample surface and that the alkyl chain is close to the surface normal as well. This is consistent with the conclusions from previous

studies and has been considered as a general characteristic of alkanethiol SAMs on gold films [43, 45, 46].

Although the heating process does not change the chemical composition of the TSBC16 SAM, it affects molecular long range order, as shown by the lattice resolved AFM images. It also produces a change in the angular dependence of the intensity of the resonance peaks in the NEXAFS measurements. The photoemission study of azobenzene alkanethiol SAMs by Weber and coworkers [16] reported that synchrotron irradiation may induce *trans-cis* isomerization. To avoid complication due to similar effects in our molecular film we choose the $\sigma^*_{C\text{-}H}$ resonance (peak 2) for a quantitative comparison of the angular dependence. This peak is a well resolved resonance that indicates the orientation of C16 in the SAMs, so we can focus on it for a detailed quantitative analysis. The intensity of this peak at different angles is shown in Figs. 4a and b, and its polarization dependence in Fig. 4d. The polarization dependence of the TSBC16SH SAM is clearly enhanced after annealing. While the peak intensity prior to annealing shows only a weak angular dependence, after annealing it shows a much larger variation reflected by the increased slope.

Fig. 5 shows the results of C-AFM measurements on the annealed sample. The lower resolution in the topographic image (Fig. 5a) is a result of the large radius of the Pt-coated tip used in this measurement (60 ± 10 nm measured from the SEM micrograph in Fig. 5e). The topographically high regions (Fig. 5a) correspond to well-packed islands. They show lower friction (Fig. 5b) and higher conductivity (Fig. 5c). As can be seen from Fig. 5d, at a sample bias of +1.8 V the current level on the islands is ~ 300 pA, while it is less than 1 pA in the surrounding disordered phase. As can be seen from Fig. 5a, the disordered phase is 3 to 4 Å lower than the islands. It is remarkable that the current level is much higher on top of the islands than on the disordered phase in between, where the tip is closer to the Au substrate. At a sample bias of -1.8 V, the current level on the islands is approximately -20 pA, one order of magnitude lower than that at +1.8 V. The molecule forms a relatively strong S-Au bond with the substrate, while only weakly interacts with the tip via the van der Waals force. On the other hand, the C16 saturated hydrocarbon chain strongly decouples the TSB unit from the substrate. It is therefore rather complicated to determine the relationship between the molecular energy levels, i.e., highest occupied molecular orbital (HOMO) and lowest unoccupied molecular orbital (LUMO), and the Fermi levels of the Au substrate and Pt tip. Although the previous study on PPV by Campbell et al. [47] suggests that conduction is mainly due to hole transport via HOMO, it is not necessarily the same case for the hybrid molecule in our study.

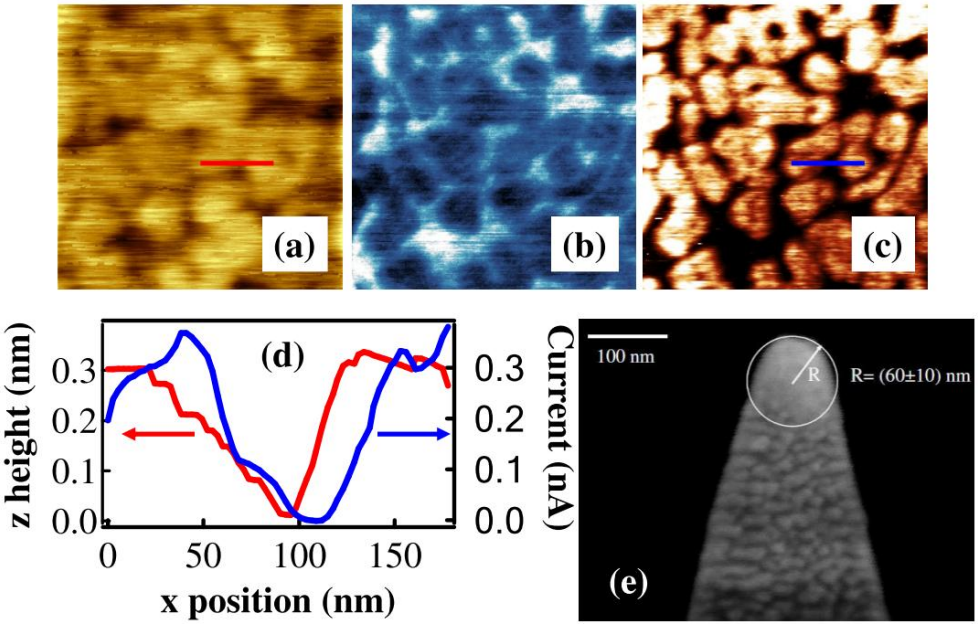

Figure 5. 680 nm × 680 nm C-AFM topographic (a), friction (b), and current (c) images (total load = 38nN, scanning speed = 1.4 μm/s, sample bias = 1.8V) of an annealed TSBC16SH SAM on Au(111). Profiles along the marked lines in (a) and (c) are shown in (d). (e) SEM micrograph of a Pt tip after AFM measurements showing a radius of (60 ± 10) nm at the tip apex.

The structure of the molecular film can be altered by scanning at a high load. The structural changes resulted in a reduction of the current level. This is most likely due to an increased degree of disorder induced by the high tip pressure. In Fig. 6a, a region of reduced current (a 700 nm × 700 nm square) can be clearly recognized. The square was previously scanned under a total load of 77 nN. The topographic height of the square region decreases by approximately 3Å relative to the surrounding region. The current on the islands outside the square is ~ 0.9 nA, while the current on islands inside the square is ~ 0.2 nA. In the friction image (Fig. 6b) that was simultaneously acquired, the sqaure region exhibits higher friction, suggesting more disorder induced by the high load scanning. Note that the very bright stripes in Fig. 6b are caused by the AFM tip moving "debris" created by previous high load scanning.

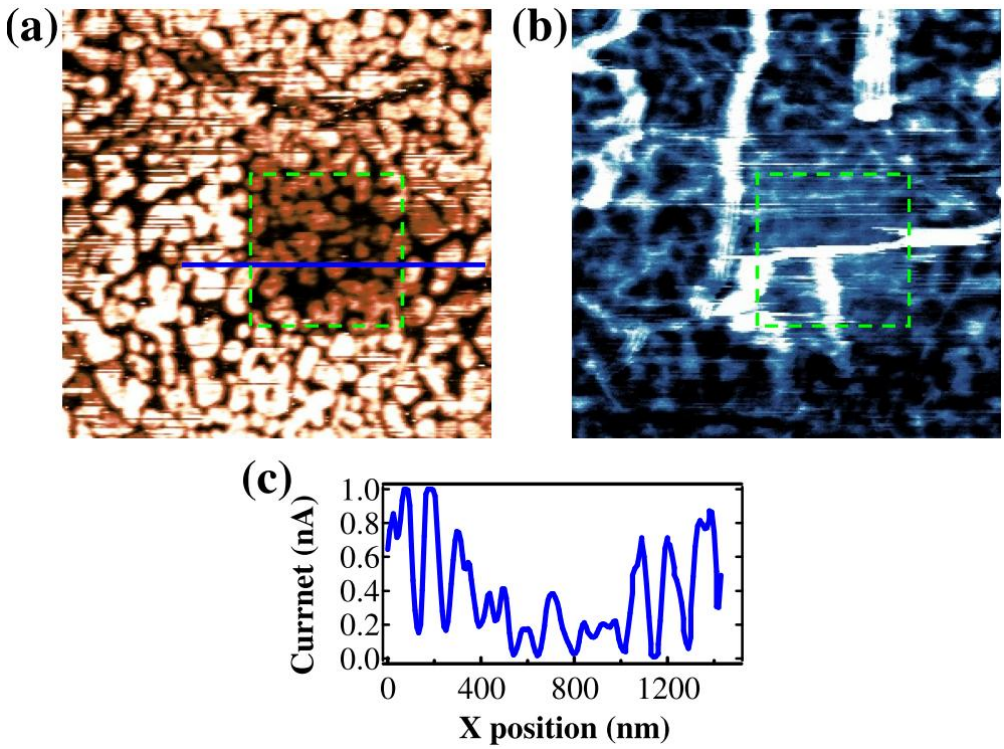

Figure 6. 2 μm × 2 μm current (a), and friction (b) images acquired in C-AFM measurements of TSBC16SH SAMs on Au (total load = 38nN, scanning speed = 4 μm/s, sample bias = 1.8V, bright = high current / friction). The region marked by a square (700 nm × 700 nm) in the image was previously scanned with a total load of 77 nN. This reduced the height of the film inside the square by ~3Å. (c) Current profile along the marked line in (a).

4. Discussion

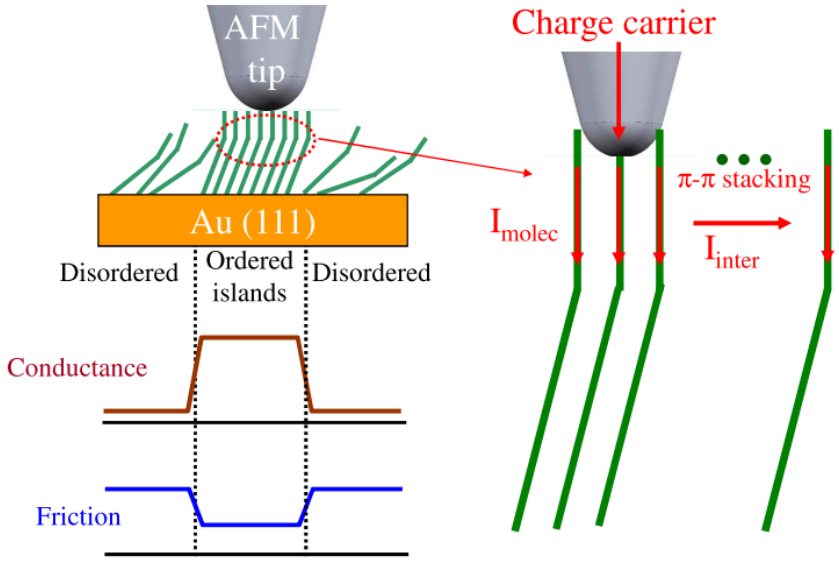

Figure 7. Schematic representations of the enhanced conductance and reduced friction of

large islands as a result of better ordering.

4.1 Non-annealed versus annealed TSBC16SH SAMs

Studies have shown that annealing the SAMs can increase the domain size and improve sample crystallinity significantly. [39,48,49] Annealing at 120°C for 1 hour produced two changes: (1) small islands change to larger, flat, crystalline islands; (2) gap regions are opened between the islands containing fewer molecules. Prior to annealing the current through TSBC16SH SAMs was very low (<1 pA). After annealing the current increases to 300 pA, i.e., at least two orders of magnitude higher. It has been reported that strong π-π interactions can enhance the conduction through SAMs with conjugated groups [1,18,50-54]. In our study, a higher degree of order, shown by the lattice resolved AFM images, is likely to lead to a better π-π stacking between the TSB units of neighboring molecules. This, we believe, is the reason for the higher conductivity on islands (Fig. 7).

4.2 Crystalline islands versus disordered phase

The disordered phase between the islands after annealing is 3 to 4 Å lower in height (Fig. 5a) and possibly lower in the case of incomplete tip penetration (finite tip radius comparable to gap width). The C-AFM study of alkanethiol SAMs from our earlier work gives a decay parameter $\beta = 0.57$ Å^{-1} when the tilt angle of hexadecanethiol molecules increases under the external force exerted by the AFM tip [55]. If the conduction mechanism of TSBC16SH were similar to that of C16SH, i.e., by tunneling along the molecular chain, a ~ 3 Å decrease in the molecule height would result in a five-fold enhancement in the current. In our study the disordered phase shows a conductivity reduced by more than two orders of magnitude. This drastic decrease is caused, we believe, by the loss of overlap between the π system of the TSB units, which plays a very important role in charge transport through and across molecules. As illustrated in Fig. 7, there are two possible conduction channels: the conduction along the molecule (I_{molec}) and the inter-molecule conduction (I_{inter}). The inter-chain conduction is only efficient when there is good π-π stacking. It is this better π-π stacking between TSB units of neighboring molecules that causes a higher conductivity on the large islands (Fig. 7). Disorder destroys efficient π-π overlap and this causes a drastic conductance reduction. This is also the reason for the reduction in current observed after high-load scanning, which causes disorder in the film (Fig. 6a). It has been reported that disorder such as gauche defects induced in SAMs comsisting of saturated alkane chains also tends to decrease charge transport efficiency [56, 57], although the magnitude of the decrease is not as significant as observed in this study.

4.3 C16SH versus TSBC16SH

Next we can compare the current level on TSBC16SH large islands to that on hexadecanethiol (C16SH) SAMs under similar conditions. The conduction mechanism through metal-molecule-metal (MMM) junctions containing simple alkanethiol SAMs is non-resonant tunneling [21]. The conduction follows an exponential decay with the number

of carbon atoms in alkanethiol molecules according to $G = G_0 \cdot e^{-\beta n}$, where G is the conductance of junction, G_0 is the contact conductance, β is a characteristic decay parameter of the system, and n is the number of carbon atoms in alkanethiol molecules. The value of β has been measured by varying the length of alkanethiols and using a variety of experimental techniques such as mercury drop electrodes [58], C-AFM [59], and nanopores [21]. All these measurements give approximately the same result $\beta \sim 1.1$/carbon.

In order to compare our C-AFM results to published data we have to determine the current density by estimating the tip-SAM contact area. For soft and adhesive materials such as SAMs, the changes in contact area can be adequately described by the Johnson-Kendall-Roberts (JKR) continuum elastic contact model [52,60]. The contact area under the imaging conditions in Fig. 5 is 59 nm^2 for our tip radius and load based on that model. This leads to a current density of 5×10^6 A/m^2. The parameters used in the calculation are: the Pt-coated tip radius R = (60 ± 10) nm (determined from the SEM micrograph in Fig. 5e), the adhesion force L_C = -20 nN (determined from the critical pull-off force), Pt Young's modulus E_1 = 140 GPa, Poisson ratio ν_1 = 0.38, Au Young's modulus E_2 = 78 GPa, Poisson ratio ν_2 = 0.44. The current density on C16SH SAMs under similar conditions (total load = 44nN and bias = 1.8V) was found to be $J = 1\times10^7$ A/m^2 by our C-AFM measurements (data not shown). Lee et al. reported a current density of C12SH SAMs with C-AFM of $J = 5\times10^8$ A/m^2 (load = 20nN and bias = 1V). [61] The extrapolation to C16SH using a decay parameter β = 1.1/carbon gives $J = 5\times10^6$ A/m^2. Similarly the extrapolation from C-AFM measurements by Wold et al. [59] gives a current density $J \sim 4\times10^6$ A/m^2 for C16SH SAMs. It is remarkable that with the additional TSB group, with a length of ~ 11 Å, the current density on the islands of TSBC16SH is of the same order of magnitude as that of hexadecanethiol (C16SH). The fact that the TSB segment does not attenuate the conductance suggests efficient electronic coupling of the coplanar phenylene units, which provides a lateral contribution to the conduction. Electronic coupling has also been proposed to explain an extremely low distance decay constant of $\beta = 0.06$ $Å^{-1}$, observed in a series of ferrocene oligophenylenevinylene methyl thiol monolayers on Au [62].

It is worth mentioning that the higher conductivity of TSBC16SH cannot be explained by a high conductance of the TSB unit of individual molecules, because the disordered phase shows a very low current level. In the disordered phase, disorder suppresses the inter-molecule conduction, and only the conduction along the molecules remains.

5. Conclusion

In conclusion, we have investigated the electrical and friction properties of ω-(*trans*-4-stilbene)alkylthiol self-assembled monolayers (SAMs) on Au(111) using atomic force microscopy (AFM) and near edge x-ray absorption fine structure spectroscopy (NEXAFS). The sample surface prior to heating was uniformly covered with a molecular film consisting of small grains (size 10 ~ 20 nm, RMS roughness 1 ~ 2 Å). Well-packed islands, with sizes between 100 and 200 nm, and RMS roughness ~ 0.5 Å, were formed after the sample was heated in a dry nitrogen gas atmosphere at 120 °C for 1 h. Lattice resolved AFM images indicate a periodic ordering in the islands, while

the areas between the islands were covered with disordered molecules with a topographical RMS roughness as high as ~ 4 Å. The ordered islands exhibit substantial reduction (50%) in friction as expected from well ordered films. The islands were ~ 6 Å higher than the surrounding disordered phase, indicating that the molecules in the islands stand more upright than in the disordered phase. NEXAFS measurements revealed a substantial increase of verticality and ordering after heating. Conductance-AFM (C-AFM) measurements revealed more than two orders of magnitude enhancement in conductivity on the islands relative to the disordered phase. We conclude that the conductance enhancement is a result of a better π-π stacking between *trans*-stilbene units of neighboring molecules as a result of improved ordering in islands. This makes possible inter-molecule conduction in addition to the tunneling conduction along the molecular chains to the gold substrate.

6. Acknowledgments

This work was performed at the Molecular Foundry, Lawrence Berkeley National Laboratory, and was supported by the Office of Science, Office of Basic Energy Sciences, Materials Science and Engineering of the U.S. Department of Energy under Contract No. DE-AC02-05CH11231. XL and FH were supported by MRSEC at the University of Wisconsin-Madison funded by NSF under DMR-0520527. XL thanks the support of an Doctoral Fellowship from the Berkeley Advanced Light Source.

Supporting Information Available: The synthesis procedure of TSBC16SH molecules. This material is available free of charge via the Internet at http://pubs.acs.org.

References

[1] Smits, E. C. P.; Mathijssen, S. G. J.; van Hal, P. A.; Setayesh, S.; Geuns, T. C. T.; Mutsaers, K. A. H. A.; Cantatore, E.; Wondergem, H. J.; Werzer, O.; Resel, R.; Kemerink, M.; Kirchmeyer, S.; Muzafarov, A. M.; Ponomarenko, S. A.; de Boer, B.; Blom, P. W. M.; de Leeuw, D. M. *Nature* **2008**, *455*, 956.

[2] Sekitani, T.; Noguchi, Y.; Hata, K.; Fukushima, T.; Aida, T.; Someya, T. *Science* **2008**, 321, *1468*.

[3] Kim, J.-S.; Lu, L.; Sreearunothai, P.; Seeley, A.; Yim, K.-H.; Petrozza, A.; Murphy, C. E.; Beljonne, D.; Cornil, J.; Friend, R. H. *J. Am. Chem. Soc.* **2008**, *130*, 13120.

[4] Andrews, D. Q.; Solomon, G. C.; Duyne, R. P. V.; Ratner, M. A. *J. Am. Chem. Soc.* **2008**, *130*, 17309.

[5] Yan, H.; Chen, Z.; Zheng, Y.; Newman, C.; Quinn, J. R.; Dotz, F.; Kastler, M.; Facchetti, A. *Nature* **2009**, *457*, 679.

[6] Miller, E. K.; Yoshida, D.; Yang, C. Y.; Heeger, A. J. *Phys. Rev. B* **1999**, *59*, 4661 .

[7] Yu, J.; Hu, D.; Barbara, P. F. *Science* **2000**, *289*, 1327.

[8] Park, L. Y.; Munro, A. M.; Ginger, D. S. *J. Am. Chem. Soc.* **2008**, *130*, 15916.

[9] Giro, R.; Caldas, M. J.; Galvao, D. S. *International Journal of Quantum Chemistry* **2005**, *103*, 588.

[10] Ruini, A.; Caldas, M. J.; Bussi, G.; Molinari, E. *Phys. Rev. Lett.* **2002**, *88*, 206403.

[11] Sension, R. J.; Repinec, S. T.; Szarka, A. Z.; Hochstrasser, R. M. *J. Chem. Phys.* **1993**, *98*, 6291.

[12] Hugel, T.; Holland, N. B.; Cattani, A.; Moroder, L.; Seitz, M.; Gaub, H. E. *Science* **2002**, *296*, 1103.

[13] Henzl, J.; Mehlhorn, M.; Gawronski, H.; Rieder, K.-H.; Morgenstern, K. *Angew. Chem., Int. Ed. Engl.* **2006**, *45*, 603.

[14] Comstock, M. J.; Levy, N.; Kirakosian, A.; Cho, J.; Lauterwasser, F.; Harvey, J. H.; Strubbe, D. A.; Frechet, J. M. J.; Trauner, D.; Louie, S. G.; Crommie, M. F. *Phys. Rev. Lett.* **2007**, *99*, 038301.

[15] Choi, B. Y.; Kahng, S. J.; Kim, S.; Kim, H.; Kim, H. W.; Song, Y. J.; Ihm, J.; Kuk, Y. *Phys. Rev. Lett.* **2006**, *96*, 156106.

[16] Weber, R.; Winter, B.; Hertel, I. V.; Stiller, B.; Schrader, S.; Brehmer, L.; Koch, N. *J. Phys. Chem. B* **2003**, *107*, 7768.

[17] Grossmannn, F.; Feng, L.; Schmidt, G.; Kunert, T.; Schmidt, R. *Europhys. Lett.* **2002**, *60*, 201.

[18] Seferos, D. S.; Trammell, S. A.; Bazan, G. C.; Kushmerick, J. G. *Proc. Natl. Acad. Sci. USA* **2005**, *102*, 8821.

[19] Danilov, A. V.; Kubatkin, S. E.; Kafanov, S. G.; Flensberg, K.; Bjornholm, T. *Nano Lett.* **2006**, *6*, 2184.

[20] Ranganathan, S.; Steidel, I.; Anariba, F.; McCreery, R. L. *Nano Lett.* **2001**, *1*, 491.

[21] Lee, T.; Wang, W.; Reed, M. A. *Ann. N. Y. Acad. Sci.* **2003**, *1006*, 21.

[22] Salmeron, M.; Neubauer, G.; Folch, A.; Tomitori, M.; Ogletree, D. F.; Sautet, P. *Langmuir* **1993**, *9*, 3600.

[23] Durig, U.; Zuger, O.; Michel, B.; Haussling, L.; Ringsdorf, H. *Phys. Rev. B* **1993**, *48*, 1711.

[24] Bhushan B.; Liu, H. *Phys. Rev. B* **2001**, *63*, 245412.

[25] Chen, J. Y.; Murphy, A. R.; Esteve, J.; Ogletree, D. F.; Salmeron, M.; Frechet, J.M.J. *Langmuir* **2004**, *20*, 7703.

[26] Bhushan, B.; Kasai, T.; Kulik, G.; Barbieri, L.; Hoffmann, P. *Ultramicroscopy* **2005**, *105*, 176.

[27] D'Acunto, M. *Nanotechnology* **2006**, *17*, 2954.

[28] Chen, J. Y.; Ratera, I.; Park, J. Y.; Salmeron, M.; *Phys. Rev. Lett.* **2006**, *96*, 236102.

[29] Shnidman, Y.; Ulman, A.; Eilers, J. E. *Langmuir* **1993**, *9*, 1071.

[30] Cyganik, P.; Buck, M.; Strunskus, T.; Shaporenko, A.; Wilton-Ely, J. D. E. T.; Zharnikov, M.; Woll, C. *J. Am. Chem. Soc.* **2006**, *128*, 13868.

[31] Agilent Technologies, Inc., Santa Clara, CA USA, Model number: 5500 AFM/SPM microscope.

[32] Veeco Probes, Camarillo, CA USA. Model number: NanoProbe NP-S.

[33] NanoAndMore USA Co., Beaufort, South Carolina, U.S.A.

[34] Sader, J.; Chon, J.; Mulvaney, P.; *Rev. Sci. Instr.* **1999**, *70*, 3967.

[35] Liang, T. T.; Azehara, H.; Ishida, T.; Mizutani, W.; Tokumoto, H. *Synth. Met.* **2004**, *140*, 139.

[36] Ulman, A. An Introduction to Ultrathin Organic Films from Langmuir-Blodgett to Self-Assembly (Academic Press, Boston, 1991).

[37] Caldwell, W. B.; Campbell, D. J.; Chen, K. M.; Herr, B. R.; Mirkin, C. A.; Malik, A.; Durbin, M. K.; Dutta, P.; Huang, K. G. *J. Am. Chem. Soc.* **1995**, *117*, 6071.

[38] Tamada, K.; Nagasawa, J.; Nakanishi, F.; Abe, K.; Ishida, T.; Hara, M.; Knoll, W. *Langmuir* **1998**, *14*, 3264.

[39] Xiao, X. D.; Wang, B.; Zhang, C.; Yang, Z.; Loy, M. M. T. *Surf. Sci.* **2001**, *472*, 41.

[40] Xiao, X. D.; Hu, J.; Charych D. H.; Salmeron, M. *Langmuir* **1996**, *12*, 235.

[41] Barrena, E.; Ocal, C.; Salmeron, M. *J. Chem. Phys.* **2000**, *113*, 2413.

[42] Barrena, E.; Kopta, S.; Ogletree, D. F.; Charych, D.; Salmeron, M. *Phys. Rev. Lett.* **1999**, *82*, 2880.

[43] Luk, Y.-Y.; Abbott, N. L.; Crain, J. N.; Himpsel, F. J. *J. Chem. Phys.* **2004**, *120*, 10792.

[44] Dhez, O.; Abe, H.; Urquhart, S. G. *J. of Electron Spectrosc. and Relat. Phenom.* **2003**, *128*, 85.

[45] Peters, R. D.; Nealey, P. F.; Crain, J. N.; Himpsel, F. J. *Langmuir* **2002**, *18*, 1250.

[46] Crain, J. N.; Kirakosian, A.; Lin, J. L.; Gu, Y.; Shah, R. R.; Abbott, N. L.; Himpsel, F. J. *J. Appl. Phys.* **2001**, *90*, 3291.

[47] Campbell, A. J.; Bradley, D. D. C.; Lidzey, D. G. *J. Appl. Phys.* **1997**, *82*, 6326.

[48] Fenter, P.; Eisenberger, P.; Liang, K. *Phys. Rev. Lett.* **1993**, *70*, 2447.

[49] Delamarche, E.; Michel, B.; Gerber, C.; Anselmetti, D.; Guntherodt, H.-J.; Wolf, H.; Ringsdorf, H. *Synth. Met.* **1994**, *10*, 2869.

[50] Inoue, A.; Mizutani, W.; Ishida, T.; Tokumoto, H. *Appl. Phys. A* **1998**, *66*, S1241.

[51] Ishida, T.; Mizutani, W.; Akiba, U.; Umemura, K.; Inoue, A.; Choi, N.; Fujihira, M.; Tokumoto, H. *J. Phys. Chem. B* **1999**, *103*, 1686.

[52] Fang, L.; Park, J. Y.; Ma, H.; Jen, A. K.-Y.; Salmeron, M. *Langmuir* **2007**, 23, 11522.

[53] Lussem, B.; Mu1ller-Meskamp, L.; Kartha1user, S.; Homberger, M.; Simon, U.; Waser, R. *J. Phys. Chem. C* **2007**, *111*, 6392.

[54] DeLongchamp, D. M.; Sambasivan, S.; Fischer, D. A.; Lin, E. K.; Chang, P.; Murphy, A. R.; Frechet, J. M. J.; Subramanian, V. *Adv. Mater.* **2005**, *17*, 2340.

[55] Qi, Y.; Ratera, I.; Park, J. Y.; Ashby, P. D.; Quek, S. Y.; Neaton, J. B.; Salmeron, M. *Langmuir* **2008**, *24*, 2219.

[56] Haran, A.; Waldeck, D. H.; Naaman, R.; Moons E.; Cahen, D. *Science* **1994**, *263*, 948.

[57] Slowinski K.; Majda, M. *J. Electroanal.Chem.* **2000**, *491*, 139.

[58] Slowinski, K.; Chamberlain, R. V.; Miller, C. J.; Majda, M. *J. Am. Chem. Soc.* **1997**, *119*, 11910.

[59] Wold, D. J.; Frisbie, C. D. *J. Am. Chem. Soc.* **2001**, *123*, 5549.

[60] Johnson, K.; Kendall, K.; Roberts, A. *Proc. R. Soc. Lond. A* **1971**, *324*,

301.

[61] Lee, T.; Wang, W.; Klemic, J. F.; Zhang, J. J.; Su, J.; Reed, M. A. *J. Phys. Chem. B* **2004**, *108*, 8742.

[62] Sikes, H. D.; Smalley, J. F.; Dudek, S. P.; Cook, A. R.; Newton, M. D.; Chidsey, C. E. D.; Feldberg, S. W. *Science* **2001**, *291*, 1519.

Table of Contents Graphic Only

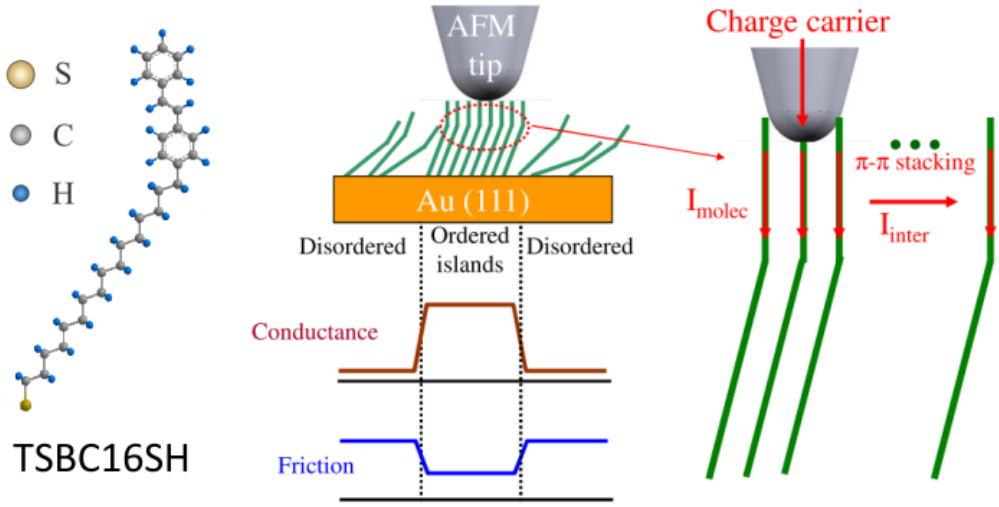
S
C
H
TSBC16SH
AFM
tip
Au (111)
Disordered
Ordered
islands
Disordered
Conductance
Friction
Charge carrier
π-π stacking
I molec
I inter